Scaling of slip weakening distance with final slip during dynamic earthquake rupture

Massimo Cocco[(1)], Elisa Tinti[(1)], Chris Marone[(1,2)], and Alessio Piatanesi[(1)]

(1) Istituto Nazionale di Geofisica e Vulcanologia, Rome, Italy

(2) Department of Geosciences, Pennsylvania State University, University Park, USA.

International Geophysics series Monograph

Fault-zone Properties and Earthquake Rupture Dynamics,

Elsevier Academic Press

Ed. Fukuyama E.

March 2009

Abstract

We discuss physical models for the characteristic slip weakening distance D_c of earthquake rupture with particular focus on scaling relations between D_c and other earthquake source parameters. We use inversions of seismic data to investigate the breakdown process, dynamic weakening, and measurement of D_c. We discuss limitations of such measurements. For studies of breakdown processes and slip weakening it is important to analyze time intervals shorter than the slip duration and those for which slip velocity is well resolved. We analyze the relationship between D_c and the parameters D_c' and D_a, which are defined as the slip at the peak slip velocity and the peak traction, respectively. We discuss approximations and limitations associated with inferring the critical slip weakening distance from D_c'. Current methods and available seismic data introduce potential biases in estimates of D_c and its scaling with seismic slip due to the limited frequency bandwidth considered during typical kinematic inversions. Many published studies infer erroneous scaling between D_c and final slip due to inherent limitations, implicit assumptions, and poor resolution of the seismic inversions. We suggest that physical interpretations of D_c based on its measurement for dynamic earthquake rupture should be done with caution and the aid of accurate numerical simulations. Seismic data alone cannot, in general, be used to infer physical processes associated with D_c although the estimation of breakdown work is reliable. We emphasize that the parameters T_{acc} and peak slip velocity contain the same dynamic information as D_c and breakdown stress drop. This further demonstrates that inadequate resolution and limited frequency bandwidth impede to constrain dynamic rupture parameters.

1. Introduction

Understanding shear traction evolution during nucleation and dynamic propagation of earthquakes is one of the major tasks for seismologists and Earth scientists. Earthquakes are the most important expression of faulting and knowledge of the processes controlling dynamic fault weakening during propagation of a seismic rupture is a crucial goal. This should be achieved by collecting geological and geophysical observations of natural faults, from laboratory experiments of friction and fracture, and by modeling seismic data and earthquake rupture using theoretical models and numerical simulations. Dynamic fault weakening can be fully described by the total shear traction evolution at a target point on the fault plane as a function of time or slip (Rice and Cocco, 2006). Figure 1 shows an example of dynamic traction, slip and slip velocity evolution as a function of time (panel a) and dynamic shear traction as a function of slip (panel b) for a target point on the fault plane; the latter is commonly called the slip weakening curve. The dynamic traction evolution of Figure 1 was obtained using a numerical procedure, discussed below, in which the rupture history derived from a kinematic inversion of seismic recordings is used as a boundary condition on the assumed fault plane (Ide and Takeo, 1997; Bouchon, 1997; Tinti et al., 2005a). We prefer to focus on dynamic traction evolution and dynamic rupture parameters that we derive from seismological observations, which allow us to constrain the rupture history including final slip, rupture time, slip duration, and details of the source time function.

Dynamic fault weakening is characterized by the stress degradation near the propagating rupture front. We discuss models in which shear stress drops from an upper yield value (τ_y) to a residual level (τ_f) in an extremely short time, called the breakdown time (T_b), and over a characteristic slip, called the slip weakening distance (D_c). The spatial extent of the breakdown zone (X_b), defined as the region of shear stress degradation near the tip of a propagating rupture, depends on the slip weakening distance. Slip velocity reaches its peak in a time T_{acc} (see Tinti et al., 2005b), corresponding to the duration of positive slip acceleration. Generally, T_{acc} is shorter or equal to the breakdown time ($T_{acc} \leq T_b$), as shown in Figure 1. Constraining slip velocity and traction evolution via analysis of seismically radiated waveforms is an extremely

important but very difficult task for modeling high frequency radiation of the earthquake source.

The seismic slip duration (i.e., the rise time) is another important parameter characterizing the rupture history and it is physically associated with healing mechanisms. In the literature, numerous studies represent dynamic rupture propagation through either a crack-like rupture mode or a self-healing pulse propagation (e.g., Cochard and Madariaga, 1994, 1996; Zheng and Rice, 1998; Cocco et al., 2004). The healing of slip, which may cause short slip durations and/or slip-velocity pulse-mode rupture propagation, has been attributed to heterogeneity of initial-stress or strength on the fault plane (e.g., Beroza and Mikumo, 1996; Bizzarri et al., 2001) or to properties of the constitutive law adopted to represent fault friction (e.g., Perrin et al., 1995; Beeler and Tullis, 1996). Self-healing ruptures have been documented during rupture propagation between dissimilar materials and in other cases (Weertman, 1980; Andrews and Ben-Zion, 1997; Cochard and Rice, 2000). Seismological models often assume a source time function of finite duration (see for instance the slip velocity plotted in Figure 1a) and therefore they may be considered more consistent with self-healing slip rather than with crack-like models. Indeed, traction evolution shown in Figure 1 exhibits restrengthening associated with healing of slip.

The purpose of this study is to elucidate the physical interpretation and seismic measurement of the characteristic slip weakening distance (D_c) with particular focus on the breakdown process and dynamic weakening. A key feature of our approach is the focus on the time scale of the breakdown process. We analyze time intervals shorter than the slip duration and ensure that periods of large slip velocity are well resolved (e.g., Figure 1).

The class of shear traction evolution models for dynamic fault weakening represented by Figure 1 are required to radiate seismic waves and to release the applied tectonic stress. Several stress parameters can be defined from the traction evolution shown in Figure 1: the strength excess ($\tau_y - \tau_o$), the dynamic stress drop ($\tau_o - \tau_f$) and the breakdown stress drop ($\tau_y - \tau_f$). Where τ_o is the initial value of stress for a particular position on the fault plane. The area below the slip weakening curve and above the residual stress level (τ_f) is traditionally identified with the fracture energy (G) (see Palmer and Rice, 1973; Andrews, 1976; Rice et al., 2005), although recently, several authors have proposed that a similar quantity called the breakdown work (W_b) is more

appropriate (Tinti et al., 2005a; Cocco et al., 2006), at least for interpreting seismological observations.

The breakdown work is a more general definition of seismological fracture energy (Cocco et al., 2006) and it is different from fracture energy as defined in classic fracture mechanics (see Abercrombie and Rice, 2005; Cocco and Tinti, 2008). The seismological breakdown work accounts for 1) the portion of the mechanical work dissipated within the fault zone, including surface area production, heat and other factors, 2) traction evolution in the pre-yield stress region, which represents the energy lost during the initial slip-hardening phase (Figure 1), and 3) the effects of spatial and temporal variations in slip direction. Because it is a more realistic representation of the earthquake process, we use the breakdown work as a proxy for seismological fracture energy in this study. The use of breakdown work also provides a means of studying spatial variations in seismological fracture energy because it can be defined at each point on the fault plane. Breakdown work represents the only measurable portion, through seismological observations, of the energy absorbed on the rupture plane for fracture and frictional dissipation (see Cocco et al., 2006). Therefore, measuring breakdown work is quite important for understanding the earthquake energy balance and for constraining the energy to be radiated as seismic waves.

In this study, we focus on the physical interpretation and measurement of the critical slip weakening distance D_c via modeling of seismological data. Our approach requires knowledge of the rupture history in order to image slip and/or slip velocity evolution and to constrain dynamic traction evolution on the fault plane. The parameter D_c is commonly measured from the same slip weakening curves (see Figure 1b) used to measure breakdown stress drop and breakdown work (or fracture energy). Recently, Mikumo et al. (2003) and Fukuyama et al. (2003) have proposed an alternative approach that allows estimation of the slip weakening distance directly from seismic observations. They proposed to measure the slip at the time of peak slip velocity, called D_c', and use this as a proxy for D_c. As shown in Figure 1a, D_c' differs from D_c and, as we will discuss later, their ratio depends on fault constitutive properties (Tinti et al., 2004). However, D_c' has been considered as a reliable approximation of D_c in some cases. Fukuyama et al. (2003) stated that this approximation works well for smoothly propagating ruptures. In this paper, we further discuss the validity of using D_c' as an alternative seismological estimate of D_c.

2. Rupture history from kinematic source models

Earthquake rupture history is often imaged through inverse approaches using a kinematic source parameterization. Geophysical data (seismograms and geodetic data) are inverted using non-linear algorithms to infer the spatiotemporal distribution of fault slip, slip direction (rake angle) and slip duration (rise time). The range of numerical approaches in use assume either an analytical source time function (single-window approach) or represent the source time function as the superposition of several triangular functions (multi-window approach) [see the detailed discussion in Cohee and Beroza, 1994]. The latter method has the advantage of avoiding the selection of an analytical source time function, but limitations include poor resolution and a sparse sampling of the slip velocity time history. On the contrary, the single window approach has the limitation of the *a priori* choice of source time function, but allows higher resolution sampling of the source time function and thus can provide better constraint on the breakdown process and the rupture history on the fault plane.

Figure 2 displays several examples of slip velocity source time functions currently adopted in the literature. They have different parameterization and for each model slip velocity reaches its peak in a different time interval. Piatanesi et al (2004) discuss the effect of using different source time functions for imaging the distribution of dynamic parameters on the fault plane (dynamic and breakdown stress drop, strength excess and critical slip weakening distance). They pointed out that the choice of the slip velocity function affects the inferred dynamic parameters; in particular, as we will discuss in the following, different source time functions yield different values of critical slip weakening distance and a different scaling with final slip.

Figure 3 shows the final slip distribution for the 1979 Imperial Valley earthquake obtained by Hartzell and Heaton (1993) by inverting strong motion data. The authors used an asymmetric triangular function having a rise time of 0.7 seconds and the time to peak slip velocity T_{acc} equal to 0.2 seconds. The five panels on the bottom display the slip and slip velocity time histories at selected positions on the fault plane indicated by letters in the upper panel. This kinematic model is an example in which the rise time is assumed constant on the fault (and therefore it is not inverted) and the slip velocity time histories have a constant shape in all subfaults and vary only in amplitude.

As noted by Piatanesi et al. (2004), the use in kinematic modelling of source time functions not compatible with the dynamic rupture propagation could bias the estimate of D_c and hence the inferred ratio of D_c to the total slip D_{tot}. Based on these results Tinti et al. (2005b) proposed the use of a new source time function to infer kinematic source models consistent with earthquake dynamics, which they named the regularized Yoffe function (shown in Figure 1a, see Tinti et al., 2005b, for the details of its analytical parameterization). Although other candidate source time functions are available in the literature (see for instance Nakamura and Miyatake, 2000; Dreger et al., 2007), we emphasize that the regularized Yoffe function is consistent with dynamic solutions of the elasto-dynamic equation (Nielsen and Madariaga, 2003) and allows a flexible parameterization for our purposes.

In order to image the rupture history on the fault plane, robust kinematic inversions have been proposed to improve resolution. A variety of smoothing constraints have been adopted to ensure stable solutions of the inverse problem (see Hartzell et al., 2007 and references therein). It is generally accepted to use positivity and smoothing constraints (Hartzell and Heaton, 1983; Henry et al., 2000, among many others) for reducing the instability and the complexity of the inverted models to levels consistent with resolution of the filtered data. However, depending on the choice of assumed spatial or temporal constraints, the results of the inversions (in terms of kinematic parameters) may change dramatically (see Beresnev, 2003). Moreover, other factors can also strongly affect results such as signal pre-processing (Boore, 2005; Boore and Bommer, 2005), model parameterization (Piatanesi et al., 2007) and inversion schemes (see Hartzell et al. 2007 and references therein). Because of the difficulties in computing accurate Green's functions at high frequencies (f > 2Hz), approaches based on waveform inversion model seismograms in a limited frequency bandwidth. Applying filters to recorded seismograms helps in imaging the slip distribution but it reduces the available resolution of the source process at small wavelengths. Spudich and Guatteri (2004) highlighted the effects of the limited frequency bandwidth of modelled data on the inferred dynamic and frictional parameters. Despite these limitations, rupture history can be retrieved only through kinematic source models, and therefore they represent a unique resource of information to better understand earthquake dynamics.

3. Inferring traction evolution

Tinti et al. (2005a) have implemented a 3-D finite difference code based on the Andrews (1999) approach to calculate the stress time histories on the earthquake fault plane from kinematic rupture models. The fault is represented by a surface containing double nodes and the stress is computed through the fundamental elastodynamic equation (Ide and Takeo, 1997; Day et al., 1998). Each node belonging to the fault plane is forced to move with a prescribed slip velocity time series, which corresponds to imposing the slip velocity as a boundary condition on the fault and determining the stress-change time series everywhere on the fault. This numerical approach does not require specification of any constitutive law relating total dynamic traction to friction. The dynamic traction evolution is a result of the calculations. The numerical model is consistent with the analytical model proposed by Fukuyama and Madariaga (1998), where stress change [$\sigma(\mathbf{x},t)$] at a position **x** of the fault plane is related to slip velocity time history [$v(\mathbf{x},t)$] at time *t* by means of the following relation:

$$\sigma(\mathbf{x},t) = -\frac{\mu}{2\beta} v(\mathbf{x},t) + \int_{\Sigma}\int_{0}^{t} K(\mathbf{x}-\xi;t-t')v(\xi,t)dt'dS \,, \qquad (1)$$

where β is the shear wave velocity, μ the shear rigidity, *K* the dynamic load associated to those points that are already slipping (that is, those within the cone of causality around the rupture front). Piatanesi et al. (2004) used the same approach to infer dynamic parameters from kinematic models.

The slip velocity time histories at each point on the fault plane are obtained from the kinematic rupture models inferred by inverting geophysical data. In order to convert the slip model to a continuously differentiable slip-rate function, the original kinematic models have to be interpolated and smoothed both in time and space (see Day et al., 1998; Tinti et al., 2005a, for details). The free surface is included in these computations and the Earth models are simplified assuming homogeneous half-spaces. As discussed above, the inadequate resolution and the limited frequency bandwidth, which characterize inverted kinematic models, reduce the ability to infer the real dynamic traction evolution everywhere on the fault plane. Many recent papers have investigated the limitations of using poorly resolved kinematic source models (Guatteri and Spudich, 2000; Piatanesi et al., 2004; Spudich and Guatteri 2004). We discuss these issues in further detail below.

Despite the limitations noted above, the methods proposed by Ide and Takeo (1997), Day et al. (1998), and Tinti et al. (2005a) provide the dynamic shear stress time histories on the fault plane. This is an important step in using seismological observations to understand the breakdown process during earthquake ruptures. Moreover, source time functions compatible with earthquake dynamics and suitable for waveform inversions are becoming commonly available (see Piatanesi et al., 2004; Tinti et al., 2005b; Dreger et al., 2007; Cirella et al., 2006). Finally, Tinti et al. (2005a and 2008) have discussed in detail the fidelity of calculations of breakdown work and D_c and concluded that, in agreement with Guatteri and Spudich (2000), the estimates of W_b are quite stable despite the limited available resolution in kinematic source models, while the D_c parameter is more difficult to constrain.

For these reasons, we use the approach of Tinti et al. (2005a) in the present study. Figure 4 shows the traction evolution as a function of slip for the 1979 Imperial Valley earthquake. Numbers along the axes represent the relative position along strike and dip on the fault plane of each target point. The intervals shown for the lower left panel indicate traction (in MPa) and slip (in m) and apply to each panel of Figure 4. From the inferred slip weakening curves we can measure the breakdown stress drop, D_c, and the breakdown work at each grid point on the fault plane. Figure 4 clearly shows high values of stress drop in correspondence to the large slip patch. The slip weakening curves also exhibit a slow weakening rate due to the smoothed source time function of the kinematic model. Figure 5 displays shear traction time histories (top panels) and the slip weakening curves (bottom panels) for the five points noted in Figure 3. As expected, the dynamic parameters of strength excess and breakdown stress drop vary over the fault plane (Figure 5). Moreover, D_c differs for different positions on the fault, varying from ~ 0.7 to 1.5 m for the selected positions. We also emphasize that the duration of the breakdown phase and the subsequent restrengthening phase vary over the fault plane, even though the rise time (0.7 s) and T_{acc} (0.2 s) are assumed to be constant.

The dynamic traction evolution curves inferred from kinematic rupture histories display an initial increase before reaching the upper yield stress value τ_y, as clearly evident in the examples shown in Figures 1 and 5. This initial slip hardening phase precedes the dynamic weakening phase and it is associated with relatively small slip amplitudes. We define D_a as the slip at the upper yield stress: Figure 1a shows that, at

least in this case, it is much smaller than both D_c' and D_c. In the framework of classic dynamic models, this initial hardening phase is associated with the strength excess and it is an important feature for modeling rupture propagation through spontaneous dynamic models. However, it is important to note that classic slip weakening models implicitly assume $D_a = 0$ This implies that the duration of initial slip hardening (T_{se}) is negligible and much shorter than the dynamic weakening phase ($T_{se} << T_{acc} \leq T_b$). It is important to note that the initial slip hardening phase has been observed in laboratory experiments (Ohnaka and Yamashita, 1989; Ohnaka, 2003) and modeled using rate – and –state friction (Bizzarri et al., 2001; Marone et al., 2008). We emphasize that the breakdown work estimates done by Tinti et al. (2005a) and Cocco et al. (2006) include both the initial slip-hardening and the subsequent slip weakening phases, and consequently their D_c estimates include a contribution from D_a.

4. Measuring D_c' from peak slip velocity

Following the approach proposed by Mikumo et al. (2003) we have measured D_c' from kinematic source model of the 1979 Imperial Valley earthquake, whose slip distribution is shown in Figure 3. Figure 6 displays the distribution of D_c' inferred from the slip history imaged by Hartzell and Heaton (1983) by inverting strong motion accelerograms. D_c' ranges between 0.5 and 1 m in the central, high slip patch; these values can be considered as a lower bound for D_c. As expected, the spatial distribution of D_c' is strongly correlated with the slip distribution. This is even more evident in Figure 7a, which shows the perfect linear scaling of D_c' with final slip D_{tot}. This scaling is simply the result of the initial hypothesis adopted in kinematic inversion of a fixed source time function (an asymmetric triangular function) with a constant rise time and T_{acc} (0.7 and 0.2 s, respectively). Therefore, in this kinematic model, the heterogeneity of inferred slip completely dictates the heterogeneity of peak slip velocity and hence D_c'.

Nowadays, thanks to computational tools, finite-fault inversions are commonly performed using non-linear formulations that allow all the kinematic parameters to be inverted (e.g., Ji et al., 2002; Delouis et al., 2002; Piatanesi et al., 2007). To account for the actual rupture complexity, slip or peak slip velocity, rupture time, rise time and slip

direction are simultaneously inverted. However, the parameter T_{acc} is usually fixed *a priori* because of data frequency bandwidth limitations and, as a consequence, strongly affects estimates of D_c'. Independent inversion for all of the kinematic parameters should produce a natural scatter of the correlation between D_c' and D_{tot}. However, there are still other problems and limitations in measuring D_c' from seismological observations. Spudich and Guatteri (2004) pointed out that low-pass filtering of strong motion seismograms can affect the estimates of D_c', because it biases the inverted rupture models causing an artificial correlation between D_c' and D_{tot}. These authors claimed that slip models derived from band-limited ground motion data might not resolve periods shorter than the breakdown time, and therefore the models do not contain periods shorter than T_{acc} ($\leq T_b$). They defined these inverted models as "temporally unresolved." This means that the process of low pass filtering ground motion data can remove information about D_c and D_c'. Spudich and Guatteri (2004) concluded that filtering ground motion data or the inferred slip models tends to bias upward the D_c values inferred from the slip weakening curves and to generate artificial correlations with final slip. The effect of filtering is to shift the peak slip velocity later in time, which means that T_{acc} is overestimated, and/or that postpeak energy is effectively repositioned to a time before the peak slip velocity (Spudich and Guatteri, 2004). These issues raise the question of whether estimates of D_c' from modeling ground motion waveforms are tenable and corroborated by data.

Yasuda et al. (2005) performed a particularly interesting test for the subject discussed here. They simulated a spontaneous dynamic earthquake rupture, by assuming constant D_c, and computed the synthetic waveforms that would be observed at actual receivers. Therefore they inverted these synthetic seismograms to image the kinematic rupture history and to constrain the slip rate function on each sub-fault. As expected, the spontaneous forward dynamic model has a spatial and temporal resolution much higher than the inverted model (nearly 10 times larger). This numerical test allows the comparison of inferred values of both D_c and D_c' with those of the target model. The results of Yasuda et al. (2005) clearly show that the D_c' values measured from the dynamically generated slip rate functions range between $0.25 \cdot D_c$ and D_c (as expected since $T_{acc} \leq T_b$). Also, for a constant D_c model (see Figure 3 in Yasuda et al. (2005)) the

inferred values of D_c' scale with final slip. These results are consistent with the findings of Tinti et al. (2004), who also demonstrate that the D_c' values measured from the inverted slip rate functions scale with final slip. The values of D_c' and D_{tot} so derived define a roughly linear scaling with slope equal to 1/2, although they exhibit larger scatter than values measured from the dynamically generated slip rate functions. Spudich and Guatteri (2004) explain the scaling $D_c' = 0.5 \cdot D_{tot}$ as a consequence of the central limit theorem: after the filtering operation, a source time function tends to a Gaussian in which half of the slip occurs before peak slip velocity. Yasuda et al. (2005) also concluded that both of their estimates of D_c' exhibit an apparent correlation with final slip.

The correlation between D_c' and final slip D_{tot} has also been obtained in other inversions of kinematic models. Figure 7b shows the scaling of D_c' with D_{tot} for the 1994 Northridge earthquake. These values derive from the calculations performed by Tinti et al. (2005a) using the kinematic model results of Wald et al. (1996). The latter authors used a multi-windows approach and the source time function consists of three overlapping isosceles triangles each with duration of 0.6 s and initiations separated by 0.4 s. This allows a rise time lasting up to 1.4 s. We show here values estimated for the dip-slip component of the slip vector (Figure 7b). D_c' exhibits a larger scatter around a linear scaling, which arises in part because in this case the slip rate function can contain multiple peaks at different times (see Figure 2 in Tinti et al., 2005a). Nevertheless, the correlation of D_c' with final slip is still evident (Figure 7b).

A conclusion from all of these models is that D_c' is an accurate estimate of D_c only if the inversion method retains information on the breakdown process. Unfortunately, this condition is not met, due to inherent limitations on spatial and temporal resolution of kinematic source models. Moreover, although one might expect to be able to use D_c' as a proxy for D_c in numerical models of dynamic rupture, it is quite difficult to constrain D_c' from the rupture history imaged from kinematic inversions because in these approaches the slip velocity function is chosen *a priori* (single window) or it is imaged with a poor resolution insufficient to resolve T_{acc}. Fukuyama et al. (2003) pointed out that also for a smoothly propagating rupture the standard deviation of the measured D_c' values can be larger than 30%. We therefore

conclude that the correlation of D_c' with final slip is often an unavoidable consequence of *a priori* assumptions and limited resolution. In the next sections we discuss i) a physical explanation of the deviation of D_c' from D_c and ii) the problem of poor resolution of the breakdown process.

5. Measuring D_c from inferred traction evolution curves

We have discussed approximations and limitations associated with inferring the critical slip weakening distance from the slip at peak slip rate. Here, we discuss the estimation of D_c directly from the slip weakening curves obtained from the inverted kinematic rupture histories. As noted above, we follow the approach proposed by Ide and Takeo (1997), Day (1998) and Tinti et al. (2005a). Figure 8 shows the D_c values inferred from the traction evolution curves displayed in Figure 4 and obtained from the slip history imaged by Hartzell and Heaton (1983) for the 1979 Imperial Valley earthquake. A visual comparison between Figures 3 and 8 suggests that D_c is correlated with final slip. This correlation is illustrated in Figure 9, which shows the scaling of D_c with final slip for all the sub-faults of this model (see Tinti et al., 2005a for details). The proportionality between D_c and final slip has been obtained by several other authors (Dalguer et al., 2003; Pulido and Kubo, 2004; Burjanek and Zaharadnik, 2007) and imaged for other earthquakes. Figure 11 of Tinti et al. (2005a) displays a similar scaling also for the 1995 Kobe and the 1997 Colfiorito earthquakes. Therefore, we conclude that, similarly to D_c', the estimates of D_c scale with final slip according to a nearly linear relationship.

Another interesting features emerges from Figure 9: it shows that most of the subfaults have a D_c value quite close to the final slip ($D_c \approx D_{tot}$). This is even more clear in Figure 10, which displays the spatial distribution of the ratio D_c/D_{tot} on the fault plane. The ratio is close to the unity over much of fault plane (Figure 10). This is due to the source time function selected for modeling observed ground motions (Piatanesi et al., 2004), and to the limited spatial and temporal resolution employed in numerical calculations (Spudich and Guatteri, 2004; Yasuda et al., 2005).

In order to better understand the effects of adopting different source time functions in retrieving dynamic traction evolution, we show in Figure 11 the dynamic traction evolution inferred for two slip rate functions:

$$f_1 = \dot{f}(t) = H(t)\frac{2}{T_R}\left[1-\tanh^2\left(\frac{2}{T_R}(2t-\frac{3}{2}T_R)\right)\right]$$
$$f_2 = \dot{f}(t) = H(T_R-t)\frac{2}{\pi\cdot T_R}\left(\frac{-t+T_R}{t}\right)^{1/2} \qquad (2)$$

where *H(t)* is the Heaveside function and T_R is the rise time. The first function f_1 is a smoothed ramp function in slip resulting in a Gaussian slip rate function; the second function f_2 is the Yoffe function, which is singular at the rupture time (see Piatanesi et al., 2004). The numerical representation of the latter is obtained by smoothing the function in time with a moving triangular window (0.37s) (see Tinti et al., 2005b for details of the analytical regularization of Yoffe function). These slip and slip rate functions are shown in panels a and b of Figure 11. Traction changes of panels c and d of Figure 11 are computed for the heterogeneous slip model shown in Figure 12a in a point with 2.7 m of final slip. This is the rupture history imaged by Iwata and Sekiguchi (2002) for the 2000 western Tottori, Japan, earthquake and it is characterized by a non-uniform slip distribution and an extremely variable rupture velocity. Figure 11 allows us to point out the main differences of slip rates and inferred traction evolution curves retrieved by using these two source time functions. To this goal, panels *e* and *f* of this figure display the slip, slip rate and shear traction time histories for the selected target point. It is evident that while T_{acc} for the Yoffe function is much shorter than the rise time, the same parameter is half of the rise time for the smoothed ramp. Moreover, function f_1 is characterized by a smooth onset of slip velocity, while in function f_2 it is quite sharp. All these features, which reflect peculiarities of the dynamics of earthquake rupture, yield quite different evolution curves. In particular, we emphasize that the Yoffe function yields: (i) a much shorter duration of breakdown process than the smoothed ramp, (ii) smaller values of D_c and D_c/D_{tot} than f_1, (iii) smaller values of D_c' than those of function f_1 (nearly half of the latter), and (iv) higher peak slip velocity values. We note that the two rupture histories used to compute the traction evolution curves illustrated in Figure 11 only differ for the selected slip rate function, while all the other parameters are the same (the rupture model is that shown in Figure 12a).

Figure 12 shows the strength excess and the dynamic stress drop distributions computed from the slip weakening curves inferred using the two source time functions defined above (f_1 and f_2) and two slip models differing only for the rupture velocity. Left panels depict the slip, strength excess and dynamic stress drop distributions for the variable rupture velocity model of Iwata and Sekiguchi (2002), while right panels display the same parameters for a uniform rupture velocity model (equal to 2.1 km/s). This figure clearly shows that, as expected, the variability of rupture velocity controls the heterogeneity of strength excess and dynamic stress drop on the fault plane, but it also shows that the adopted source time function affects the values of these dynamic parameters. This is in agreement with Guatteri and Spudich (2000) who concluded that there is a trade-off between strength excess and D_c in controlling the rupture velocity.

6. Scaling between D_c and final slip

In previous sections we have discussed estimation methods of both D_c' and D_c as well as the reliability of their scaling with final slip. The main limitations arise from: 1) limitations in our ability to model seismic waveforms given the narrow frequency bandwidths available (i.e., lack of high frequency components, see Spudich and Guatteri, 2004 and references therein), 2) adoption of source time functions that are not compatible with dynamic rupture propagation (see Piatanesi et al., 2004), and 3) the lack of causality constraints on spatial and temporal evolution of slip velocity in seismic inversions (i.e., poor constraints on spatial gradient of slip velocity, see Tinti et. al, 2008 for details). The duration of the breakdown process and the peak slip velocity depend on the frictional and constitutive properties of the fault. Therefore, we expect that differences between T_{acc} (timing of peak slip velocity) and T_b (breakdown duration) – and consequently between D_c' and D_c – is controlled by the constitutive properties of the source. Tinti et al. (2004) have discussed the difference between D_c' and D_c for a 2-D rupture governed by either a slip weakening or a rate- and state-dependent friction law. They demonstrated that such a difference is controlled by the strength parameter S (i.e., the ratio between strength excess and dynamic stress drop). These authors have also shown that the rate dependence of the friction law affects slip acceleration and the slip weakening parameter.

We have discussed several interpretations of the biases affecting estimates of the slip weakening distance D_c. However, the most important issue concerns the scaling of this parameter with the final slip. Although we cannot exclude the possibility that such a scaling might be physically tenable for real earthquakes, we present evidence showing that the inferred proportionality between D_c and D_{tot} is artificial. The same is true for the parameter D_c', whose estimate from kinematic slip models is controlled by the adopted source time function and by other *a priori* assumptions when inverting ground motion data. Tinti et al. (2005b) performed several simulations using a Yoffe function to represent slip velocity time history and the traction at split nodes approach to retrieve dynamic shear traction changes caused by coseismic slip. These authors propose that the following relation holds:

$$D_c \propto \sqrt{\frac{T_{acc}}{T_R}} D_{tot}\,, \tag{3}$$

suggesting that, when the duration of positive slip acceleration T_{acc} (i.e., time of peak slip velocity) and the rise time T_R are both constant or their ratio is constant, there is a direct proportionality between slip weakening distance and final slip. The values of T_{acc} and T_R control peak slip velocity, and therefore the same factors, which bias the estimate of D_c, explain the difficulties in constraining both final slip and slip velocity.

These findings are summarized in Figure 13 which shows the dynamic traction changes (panels *c*, *d*, *e* and *f*) computed for source models having a uniform slip of 1 m with a constant rupture velocity of 2.0 km/s and a slip velocity time history represented by a Yoffe function (panels *a* and *b*). Left panels display the results of calculations obtained for different T_{acc} values and a constant rise time (1.0 s), while right panels show those computed for different rise times and a constant T_{acc} equal to 0.225 s (see Tinti et al., 2005b for further details about these calculations). Panels *g* and *h* show the scaling of peak slip velocity with D_c for the two test cases. The dynamic traction histories and the slip weakening curves displayed in Figure 13 clearly illustrate that D_c and the weakening rate vary with the parameter T_{acc}. Inverting ground motion data with a limited temporal resolution overestimates the real T_{acc} and consequently produces an overestimate of D_c. The weakening rate varies in order to maintain the same value of the final slip. As a consequence, the peak slip velocity decreases for increasing T_{acc} and

D_c, as clearly shown in panel g of Figure 13. The effect of using different rise times for the same T_{acc} is to affect the D_c value, but very smoothly affecting the weakening rate. Figure 13 points out that increasing the rise time causes both D_c and peak slip velocity to decrease. Figure 13 summarizes in a simple way all the difficulties in imaging dynamic traction evolution and measuring the slip weakening parameters. It is also useful to illustrate in a schematic way all the limitations in measuring the slip weakening parameters by modeling observed ground motion data.

7. Discussion and Concluding Remarks

We discuss physical models for the characteristic slip weakening distance D_c and the scaling between D_c and total slip. We show that current methods and available seismic data introduce potential biases in estimates of D_c and its scaling with seismic slip due to the limited frequency bandwidth considered during typical kinematic inversions. For studies of dynamic slip weakening it is important to analyze time intervals shorter than T_{acc} and T_b in order to obtain accurate estimates of D_c and its scaling with total slip. Unfortunately, T_{acc} is usually fixed *a priori* in kinematic inversions due to poor data resolution. The same is true for the rise time, which is poorly constrained in kinematic inversions and often assumed to be spatially uniform on the fault plane. Therefore, in such cases, T_{acc} (and T_{acc}/T_R) strongly affect estimates of D_c' as well as D_c, and, as shown in equation (3), this generates artificial correlation of D_c with final slip. In this study, we extend previous works (Guatteri and Spudich, 2000; Tinti et al. 2008) and show that D_c inferred through seismological data can be biased unless a proper modeling of high frequency waves and source parameterization are adopted. Fukuyama and Mikumo (2007) estimated the slip weakening distance from seismograms recorded at near field stations. These authors claimed that the proposed approach is not significantly affected by spatio-temporal smoothing and resolution limitations. However, this approach also depends on several "a priori" assumptions concerning the rupture history (rupture velocity, rise time, etc…) and source time function.

We cannot exclude the existence of physical mechanisms controlling the scaling of D_c with final slip D_{tot}. Ohnaka and Yamashita (1999) and Ohnaka (2003) suggest that D_c scales with the roughness of the fault plane in the direction of slip and that D_c

has a fractal distribution on the fault plane. The idea that D_c scales with fault maturity was also proposed by Marone and Kilgore (1993) and Abercrombie and Rice (2005). On the other hand, Scholz (1988) argued that rough fault surfaces under lithostatic load will develop a characteristic contact dimension and hence exhibit a constant value of D_c, rather than one that scales with roughness (see also Brown and Scholz, 1985; Aviles et al., 1987; Power et al., 1987). Nevertheless, the assumption of a fractal distribution of D_c and the scaling with fault roughness might imply a scaling with final slip. Moreover, because slip is heterogeneously distributed on the fault plane, constant D_c models are not physically consistent (that is, they could predict D_c values larger than final slip in locked patches). A full discussion of the physical mechanisms that could yield causal scaling between D_c and final slip is beyond the scope of the present study. We emphasize that the linear scaling between D_c and D_{tot} inferred from kinematic source models is caused by the poor resolution of the breakdown process.

In this study we have shown that the estimates of breakdown work from kinematic source models are more reliable. The breakdown work is a more appropriate quantity for assessing the earthquake energy budget than the fracture energy as defined in classic fracture mechanics (Cocco et al., 2006; Cocco and Tinti, 2008). Figure 14 shows the distribution of W_b (J/m^2) obtained by Tinti et al. (2005a) for a kinematic model of the 1979 Imperial Valley earthquake (Hartzell and Heaton, 1983). The spatial distribution of breakdown work is strongly correlated with the slip distribution (see Figure 3). The correlation between the distributions of W_b and slip is due primarily to the correlation of D_c with slip, but also secondarily to the correlation of stress drop with total slip.

The two fundamental parameters characterizing dynamic fault weakening, breakdown work W_b and slip weakening distance D_c, are intrinsically scale dependent (Ionescu and Campillo, 1999; Ohnaka and Yamashita, 1989; Cocco and Tinti, 2008). This means that they cannot be associated with any other physical process controlling dynamic fault weakening at time and length scales smaller than that selected for the macroscopic representation implicit in seismological observations (see Cocco et al., 2006; Cocco and Tinti, 2008). Thus, the interpretation of the D_c estimates inferred from seismological data are representative of the macroscopic scale in which the fault zone is shrunk to a virtual mathematical plane of zero thickness. Therefore, they cannot be easily compared with estimates retrieved from laboratory experiments on rock friction

and fracture or from those associated with weakening mechanisms occurring at time and length scales smaller than the fault zone thickness.

The results of this study point out that the parameter T_{acc} and peak slip velocity contain the same dynamic information as breakdown stress drop and D_c. The inadequate resolution and the limited frequency bandwidth, which characterize inverted kinematic models, reduce the ability to infer the real dynamic traction evolution everywhere on the fault plane. Future attempts to model high frequency seismic waves are important and will be aided by high performance computing facilities and high quality seismic waveforms from borehole seismometers.

References

Abercrombie, R.E., and J.R. Rice, (2005), Can observations of earthquake scaling constrain slip weakening? , *Geophys. J. Int.*, 162, 406-424.

Andrews, D. J., (1976), Rupture propagation with finite stress in antiplane strain, *J. Geophys. Res.*, 81, 3575-3582.

Andrews, D. J., (1999), Test of two methods for faulting in finite-difference calculations, *Bull. Seismol. Soc. Am.*, 89(4), 931-937.

Andrews D.J., and Ben-Zion Y., (1997),Wrinkle-like slip pulse on a fault between different materials, *J. Geophys. Res.*,102 (B1): 553-571.

Aviles, C.A., and C.H. Scholz, (1987), Fractal analysis applied to characteristic segments of the San Andreas fault, *J. Geophys. Res.*,92 (B1), 331-344.

Beroza G.C., and Mikumo T, (1996), Short slip duration in dynamic rupture in the presence of heterogeneous fault properties, *J. Geophys. Res.*,101 (B10), 22449-22460.

Beeler N.M., and Tullis T.E., (1996), Self-healing slip pulses in dynamic rupture models due to velocity-dependent strength, *Bull. Seismol. Soc. Am.*, 86 (4): 1130-1148.

Beresnev, I. A. (2003). Uncertainties in finite-fault slip inversions: to what extent to believe? (A critical review), *Bull. Seism. Soc. Am.*, 93, 2445–2458.

Bizzarri A., M. Cocco, D.J. Andrews, and E. Boschi, (2001), Solving the dynamic rupture problem with different numerical approaches and constitutive laws, *Geophys. J. Int.*, 144 (3): 656-678.

Boore D.M., (2005), On pads and filters: Processing strong-motion data, *Bull. Seism. Soc. Am.*, 76, 368-369.

Boore, DM, and J.J. Bommer, (2005), Processing of strong-motion accelerograms: needs, options and consequences, *Soil Dynamics and Earthquake Engineering*, 25, 93-115.

Bouchon, M., (1997), The state of stress on some faults of the San Andreas system as inferred from near-field strong motion data, *J. Geophys. Res.*,102(B6), 11731-1744.

Brown, S. R. and C. H. Scholz, (1985). Broad bandwidth study of the topography of natural rock surfaces, *J. Geophys. Res.*, 90, 12,575-12,582.

Burjanek J., and J. Zaharadnik, (2007), Dynamic stress field of a kinematic earthquake source model with k-squared slip distribution, *Geophys. J. Int.*, 171 (3): 1082-1097.

Cirella, A., A. Piatanesi, E. Tinti, and M. Cocco (2006), Dynamically consistent source time functions to invert kinematic rupture histories, Eos, Trans. AGU, 87(52), Fall Meet. Suppl., Abstract S41B-1323.

Cocco, M., A. Bizzarri, and E. Tinti (2004). Physical interpretation of the breakdown process using a rate- and state-dependent friction law, *Tectonophysics* 378, 241–262.

Cocco, M., Spudich P. and E. Tinti, (2006), On the mechanical work absorbed on faults during earthquake ruptures, in Earthquakes: Radiated Energy and the Physics of Faulting, Geophysical Monograph Series 170, American Geophysical Union, 10.1029/170GM24.

Cocco M. and E. Tinti, (2008), Scale dependence in the dynamics of earthquake propagation: evidence from seismological and geological observations, submitted to *Earth Planet. Sci. Lett.*

Cochard A. and R. Madariaga, (1994), Dynamic faulting under rate-dependent friction, *Pure and Applied Geophysics*, 142, (3-4), 419-445.

Cochard A. and R. Madariaga, (1996), Complexity of seismicity due to highly rate-dependent friction, *J. Geophys. Res.*,101(B11), 25321-25336.

Cochard A. and J.R. Rice, (2000), Fault rupture between dissimilar materials: Ill-posedness, regularization, and slip-pulse response, *J. Geophys. Res.*,105 (B11), 25891-25907.

Cohee, B. P., and G. C. Beroza (1994). A comparison of two methods for earthquake source inversion using strong motion seismograms, *Ann. Geophys.* 37, 1515–1538.

Dalguer L.A., Irikura K., and J. D. Riera JD, (2003) Generation of new cracks accompanied by the dynamic shear rupture propagation of the 2000 Tottori (Japan) earthquake, *Bull. Seismol. Soc. Am.*, 93 (5): 2236-2252.

Day, S. M., G. Yu and D. J. Wald (1998) Dynamic stress changes during earthquake rupture, *Bull. Seismol. Soc. Am.*, 88, 512-522.

Delouis, B., D. Giardini, P. Lundgren, and J. Salichon (2002), Joint inversion of Insar, GPS, teleseismic and strong-motion data for the spatial and temporal distribution of earthquake slip: application to the 1999 Izmit mainshock, *Bull. Seismol. Soc. Am.*, 92(1), 278–299.

Dreger D., Tinti E and A. Cirella, (2007), Slip Velocity Parameterization for Broadband Ground Motion Simulation, Abstract for the *Annual Meeting of Seismological Society of America*.

Fukuyama, E. and R. Madariaga (1998) Rupture dynamics of a planar fault in a 3D elastic medium: Rate-and slip-weakening friction, *Bull. Seismol. Soc. Am.*, 88, 1-17.

Fukuyama, E., T. Mikumo, and K. B. Olsen, (2003), Estimation of the critical slip-weakening distance: Theoretical background, *Bull. Seismol. Soc. Am.*, 93,1835-1840.

Fukuyama, E., and T. Mikumo, (2007), Slip-weakening distance estimated at near-fault stations, *Geophys. Res. Lett.*, 34, doi:10.1029/2006GL029203.

Guatteri, M. and P. Spudich, (2000), What can strong-motion data tell us about slip-weakening fault-friction laws?, *Bull. Seismol. Soc. Am.*, 90, 98-116.

Hartzell, S., and T. H. Heaton (1983). Inversion of strong ground motion and teleseismic waveform data for the fault rupture history of the 1979 Imperial Valley, California, earthquake, *Bull. Seism. Soc. Am.*,73,1553–1583.

Hartzell, S., P. Liu, C. Mendoza, C. Ji, and K. M. Larson, (2007), Stability and uncertainty of finite-fault slip inversions: application to the 2004 Parkfield, California, earthquake, *Bull. Seism. Soc. Am.*,97,1911-1934.

Henry C, S. Das, and Woodhouse JH, (2000), The great March 25, 1998, Antarctic Plate earthquake: Moment tensor and rupture history, *J. Geophys. Res.*, 105 (B7), 16097-16118.

Ide, S. and M. Takeo, (1997), Determination of constitutive relations of fault slip based on seismic wave analysis, *J. Geophys. Res.*, 102(B12), 27379-27391.

Ionescu, I.R., Campillo M., (1999), Influence of the shape of the friction law and fault finiteness on the duration of initiation, *J. Geophys. Res.*, 104 (B2), 3013-3024.

Iwata, T., and H. Sekiguchi (2002), Source process and near-source ground motion during the 2000 Tottori-ken-Seibu earthquake, Proc. 11th Japan Earthq. Eng. Symp., 125–128.

Ji, C., D. J. Wald, and D. V. Helmberger (2002), Source description of the 1999 Hector Mine, California, earthquake, Part I: Wavelet domain inversion theory and resolution analysis, *Bull. Seismol. Soc. Am.*, 92(4), 1192–1207.

Marone C., M. Cocco, E. Richardson, and E Tinti, (2008), Mechanics of the critical slip distance for seismic and aseismic faulting, *Submitted to Special Issue of Pageoph*.

Marone C. and B. Kilgore, (1993), Scaling of the critical slip distance for seismic faulting with shear strain in fault zones, *Nature*, 362, 618-621.

Mikumo, T., K. B. Olsen, E. Fukuyama and Y. Yagi, (2003), Stress-breakdown time and slip-weakening distance inferred from slip-velocity functions on earthquake faults, *Bull. Seismol. Soc. Am.*, 93(1), 264-282.

Nakamura, H., and T. Miyatake (2000) An approximate expression of slip velocity time functions for simulation of near-field strong ground motion, *Zisin* (*J. Seism. Soc. Jpn.*), 53, 1-9 (in Japanese with English abstract).

Nielsen, S., and R. Madariaga, (2003), On the self-healing fracture mode, *Bull. Seismol. Soc. Am.*, 93(6), 2375-2388.

Ohnaka, M. (2003) A constitutive scaling law and a unified comprehension for frictional slip failure, shear fracture of intact rock, and earthquake rupture, *J. Geophys. Res.*, 108(B2), 2080, doi:10.1029/2000JB000123.

Ohnaka, M., Yamashita, T., (1989), A cohesive zone model for dynamic shear faulting based on experimentally inferred constitutive relation and strong motion source parameters. *J. Geophys. Res.*, 94, 4089–4104.

Palmer, A. C., J. R. Rice, (1973), The growth of slip surfaces in the progressive failure of over-consolidated clay. *Proc. R. Soc. London* Ser. A 332, 527-548.

Perrin, G., Rice, J.R., Zheng, G., (1995), Self-healing slip pulse on a frictional surface. *J. Mech. Phys. Solids*, 43, 1461– 1495.

Piatanesi, A., E. Tinti, M. Cocco and E. Fukuyama, (2004), The dependence of traction evolution on the earthquake source time function adopted in kinematic rupture models, *Geophys. Res. Lett.*, 31, doi:10.1029/2003GL019225.

Piatanesi, A., A. Cirella, P. Spudich, and M. Cocco (2007), A global search inversion for earthquake kinematic rupture history: Application to the 2000 western Tottori, Japan earthquake, *J. Geophys. Res.*, 112, B07314, doi:10.1029/2006JB004821.

Power, W.L., T.E. Tullis, S.R. Brown, G.N. Boitnott, and C.H. Scholz, (1987), Roughness of natural fault surfaces, *Geophys. Res. Lett.*, 14, 29-32.

Pulido, N. and T. Kubo (2004), Near-fault strong motion complexity of the 2000 Tottori earthquake (Japan) from a broadband source asperity model, *Tectonophysics*, 390, 177-192.

Rice, J.R., C.G. Sammis and R. Parsons, (2005), Off-fault secondary failure induced by a dynamic slip-pulse, , *Seismol. Soc. Am. Bull.*, 95(1), 109–134.

Rice, J. R., and M. Cocco, 2006, Seismic fault rheology and earthquake dynamics, Dahlem Workshop on *The Dynamics of Fault Zones*, pp.99-137, edited by M. R. Handy, MIT Press, Cambridge, Mass.

Scholz C.H., (1988), The critical slip distance for seismic faulting, Nature, 336, 22-29.

Spudich, P., and M. Guatteri, (2004), The effect of bandwidth limitations on the inference of earthquake slip-weakening distance from seismograms, *Bull. Seismol. Soc. Am.*, 94, 2028-2036

Tinti, E., A. Bizzarri, A. Piatanesi, and M. Cocco (2004), Estimates of slip weakening distance for different dynamic rupture models, *Geophys. Res. Lett.*, 31, L02611, doi:10.1029/2003GL018811.

Tinti, E., P. Spudich, and M. Cocco, (2005a), Earthquake fracture energy inferred from kinematic rupture models on extended faults, *J. Geophys. Res.*, 110, B12303, doi: 10.1029/ 2005JB00364

Tinti, E., E. Fukuyama, A. Piatanesi and M. Cocco, (2005b), A kinematic source time function compatible with earthquake dynamics, *Bull. Seismol. Soc. Am.*, 95(4), 1211–1223.

Tinti, E., M. Cocco, E. Fukuyama, and A. Piatanesi, (2008), Dependence of slip weakening distance (Dc) on final slip during dynamic rupture of earthquakes, submitted to *Geophys. J. Int.*

Zheng, G., and J. R. Rice (1998). Conditions under which velocity-weakening friction allows a self-healing versus a crack-like mode of rupture, *Bull. Seism. Soc. Am.*, 88, 1466–1483.

Yasuda T., Y. Yagi, T. Mikumo, T. Miyatake, (2005), A comparison between Dc'-values obtained from a dynamic rupture model and waveform inversion, *Geophys. Res. Lett.*, 32, L14316, doi:10.1029/2005GL023114.

Wald, D.J., T.H. Heaton, and K.W. Hudnut, (1996), The slip history of the 1994 Northridge, California, earthquake determined from strong-motion, teleseismic, GPS, and leveling data, Seismol. Soc. Am. Bull., 86 (1, Part B Suppl.), 49-70.

Weertman J., (1980), Crack tip advance model in fatigue of ductile material, Journal of Metals, 32, (12), 75-75.

Figure Captions

Figure 1: (*a*) Comparison of slip velocity, slip and traction time histories at a target point on a fault plane using a smoothed Yoffe function as a source time function. Black solid circle indicates the time of peak slip velocity (T_{acc}) and the grey solid circle indicate the end of weakening (T_b); (*b*) corresponding traction versus slip behavior; the same circles of panel *a* are indicated in term of slip with D_a , D_c' and D_c parameters, respectively.

Figure 2: Several analytical source time functions proposed in the literature to model the slip velocity evolution on the fault plane: Delta, Box-car, Triangular, Gaussian, Kostrov and Yoffe functions.

Figure 3: Upper panel: Slip distribution of kinematic model by Hartzell and Heaton (1983) for the 1979 Imperial Valley earthquake. Bottom panel: slip velocity and slip time histories for five subfaults as indicated by the capital letters above.

Figure 4: Traction versus slip curves of the 1979 Imperial Valley earthquake for several subfaults. The relative position on the fault plane (dip and strike) is indicated for each subfault. The intervals shown for the lower left panel ([0 2], [-20 20]) indicate traction (in MPa) and slip (in m) and are the scales for each panel.

Figure 5: Upper panel: Traction change time histories and traction change versus slip curves for the same five subfaults of Figure 3.

Figure 6: D_c' distribution for the 1979 Imperial Valley earthquake inferred from the kinematic model of Hartzell and Heaton (1983).

Figure 7a: D_c' versus total slip (D_{tot}) for all subfaults of the 1979 Imperial Valley earthquake using the Hartzell and Heaton (1983) kinematic model.

Figure 7b: D_c' versus total slip (D_{tot}) for all subfaults of 1994 Northridge earthquake using the Wald et al. (1996) kinematic model. Values are measured following the interpolation strategy discussed by Tinti et al. (2005a).

Figure 8: D_c distribution for 1979 Imperial Valley earthquake using the Hartzell and Heaton (1983) kinematic model as a boundary condition to compute traction history.

Figure 9: D_c versus total slip (D_{tot}) for all subfaults of the 1979 Imperial Valley earthquake using the Hartzell and Heaton (1983) kinematic model as boundary condition of the traction change.

Figure 10: D_c/D_{tot} distribution for the 1979 Imperial Valley earthquake using the Hartzell and Heaton (1983) kinematic model.

Figura 11: Top panel: comparison of slip (*a*), slip velocity (*b*), traction evolution (*c*) and traction versus slip curves (*d*) at a target point for the two source time functions f_1 (in black) and f_2 (in gray). Bottom panel: normalized time histories of slip, slip velocity and dynamic traction calculated with Tanh function (*e*) and Yoffe function (*f*) for the same target point.

Figure 12: Distribution of slip and rupture time (*a, f*); strength excess (*b ,c, g, h*) and dynamic stress drop (*d, e, i, l*) on the fault plane retrieved for the two source time function f_1 and f_2 and for heterogeneous (left panels) and constant (right panels) rupture velocity models.

Figure 13: The dynamic traction changes (panels *c, d, e* and *f*) for source models having uniform slip of 1 m, constant rupture velocity (2.0 km/s) and slip velocity time histories represented by Yoffe function (panels *a* and *b*). Left panels: calculations obtained for different T_{acc} values and constant rise time (1.0 s); right panels: calculations for different rise times and a constant T_{acc} (0.225s).

Figure 14: W_b distribution (J/m^2) of the 1979 Imperial Valley earthquake using the Hartzell and Heaton (1983) kinematic model.

Figures:

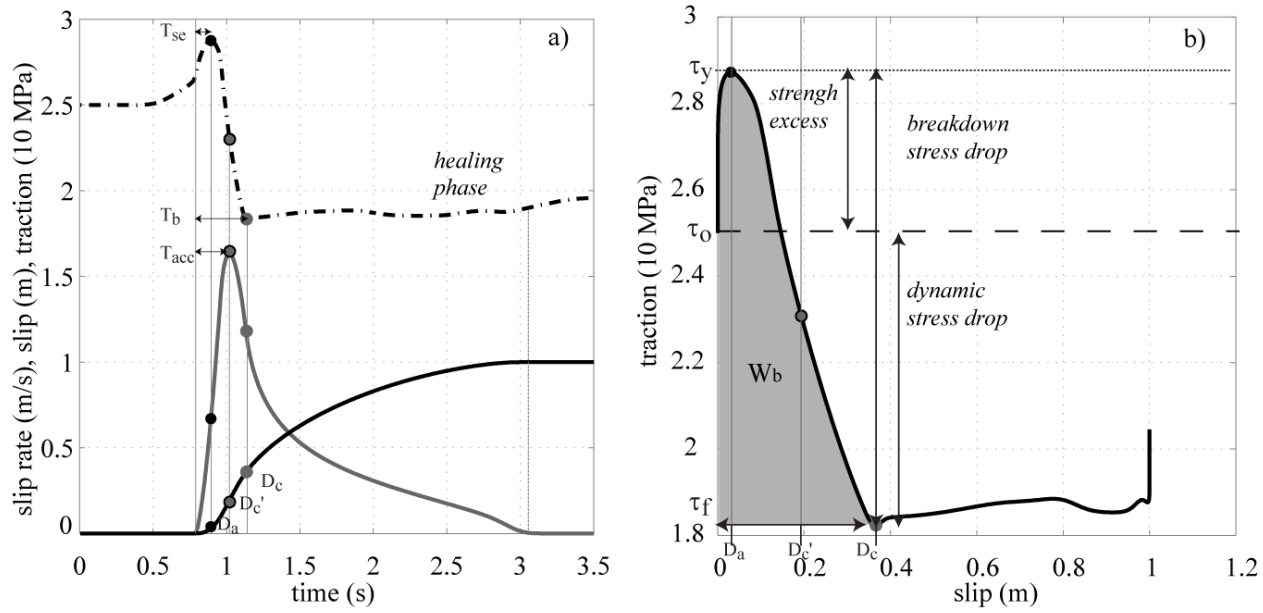

Figure 1

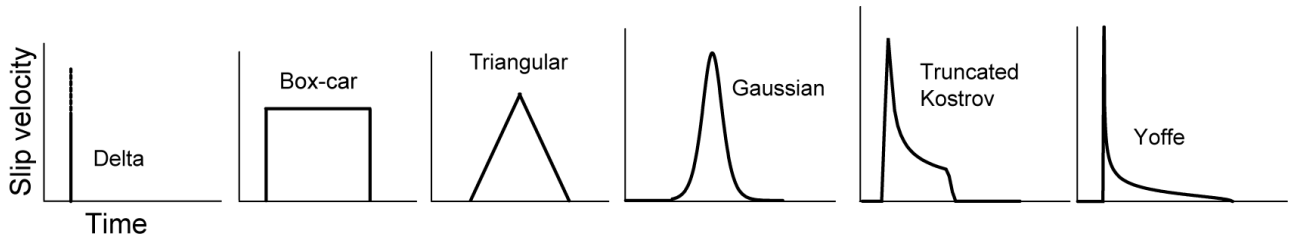

Figure 2

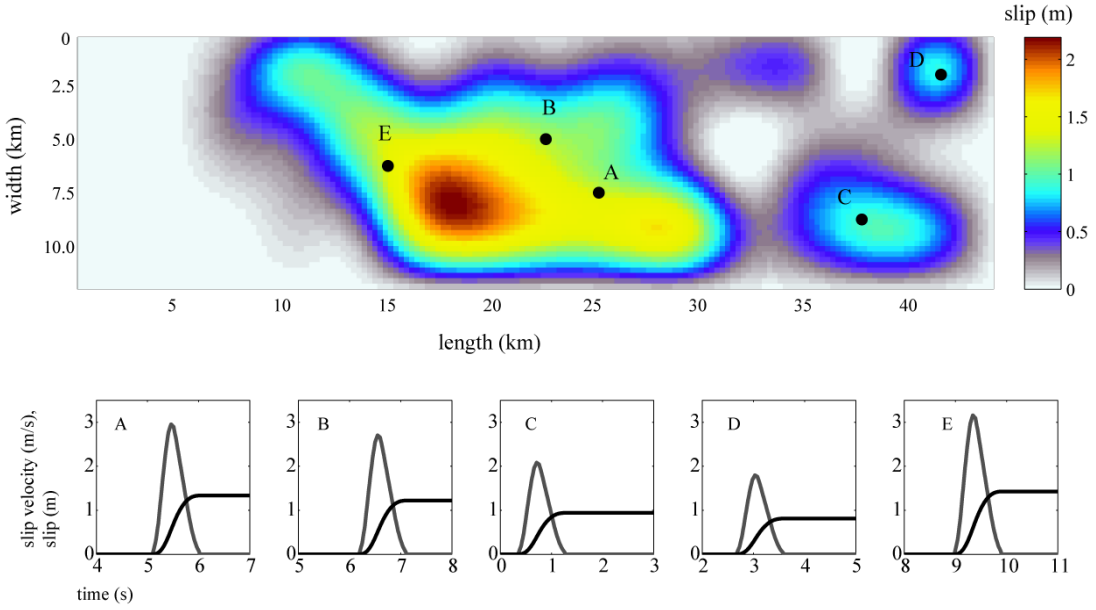

Figure 3

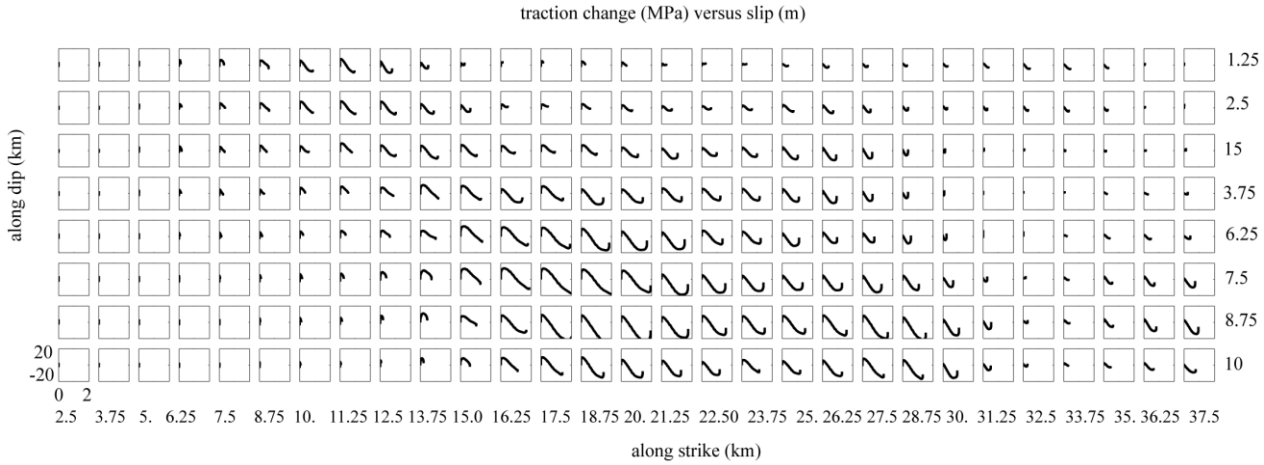

Figure 4

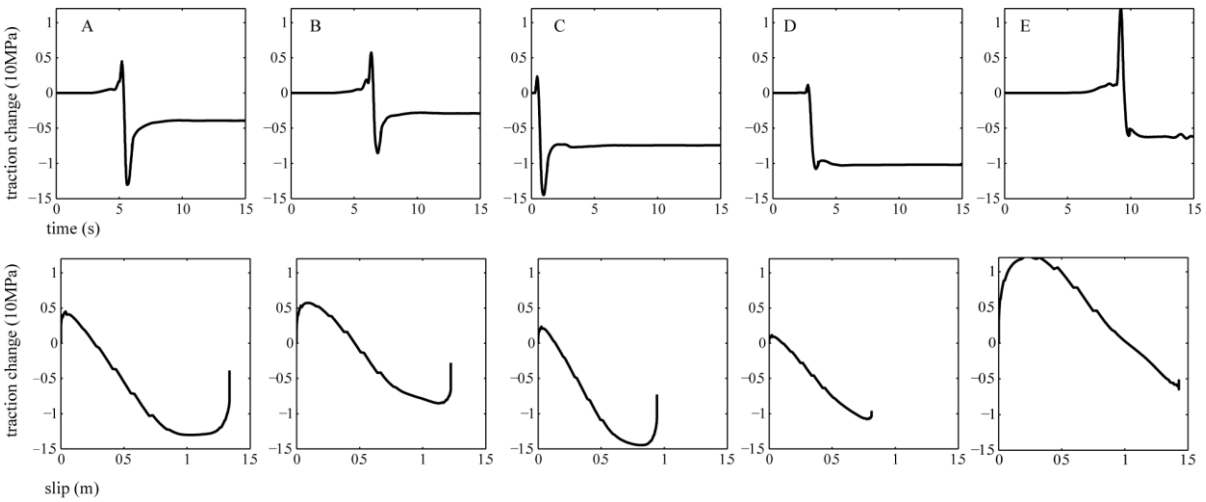

Figure 5

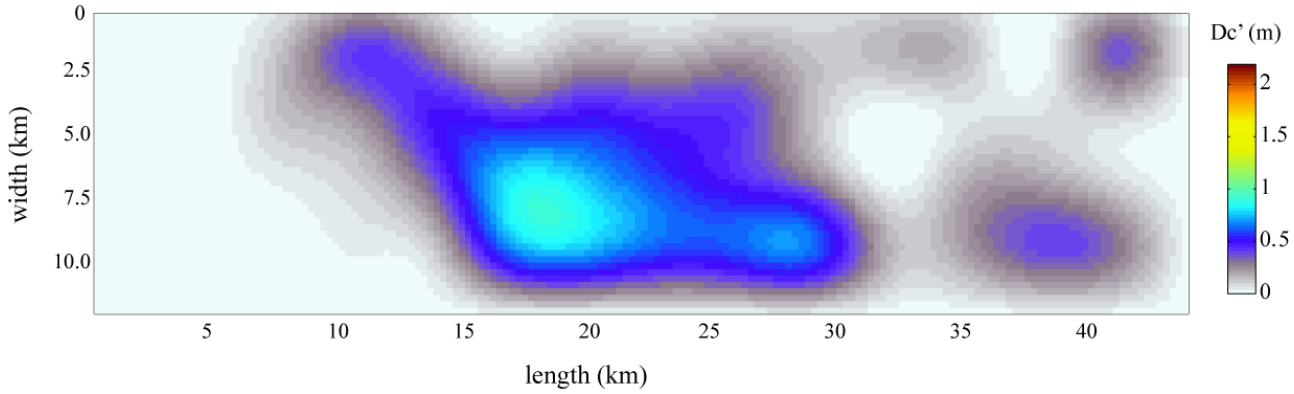

Figure 6

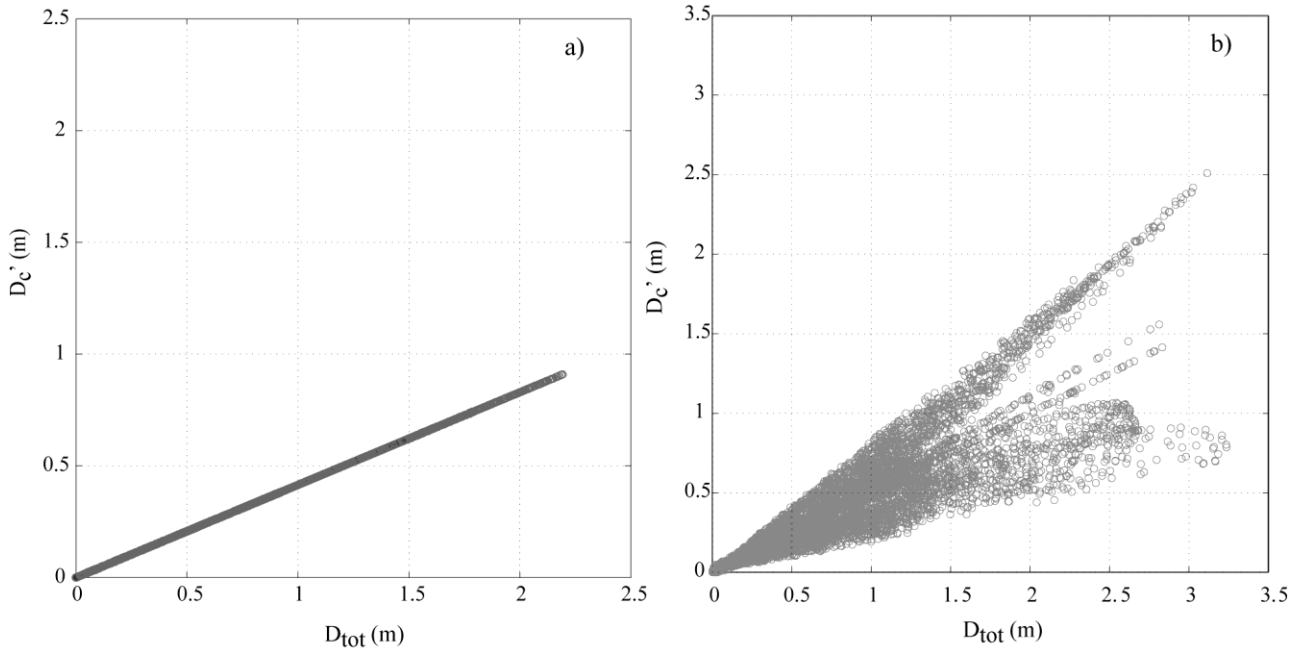

Figure 7

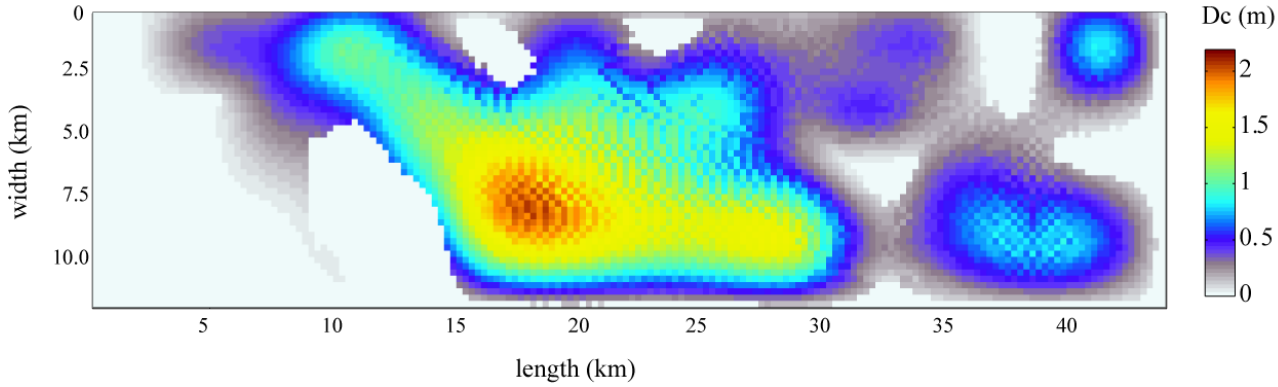

Figure 8

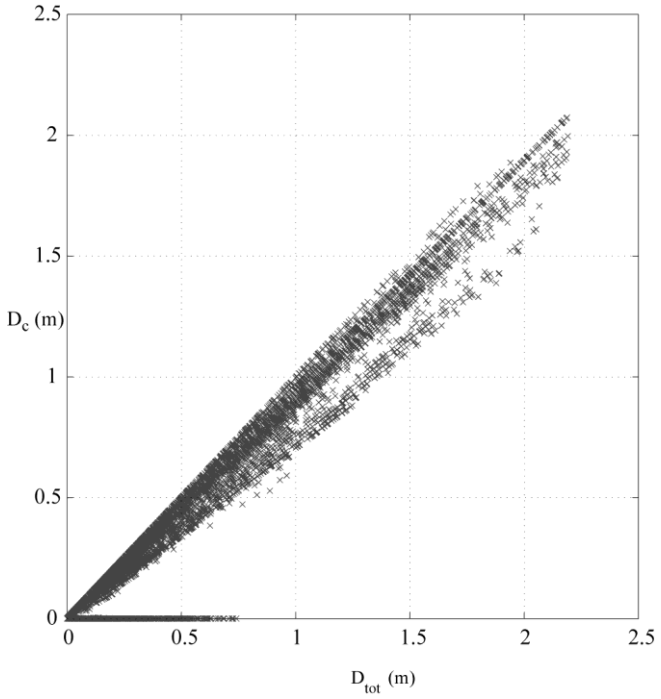

Figure 9

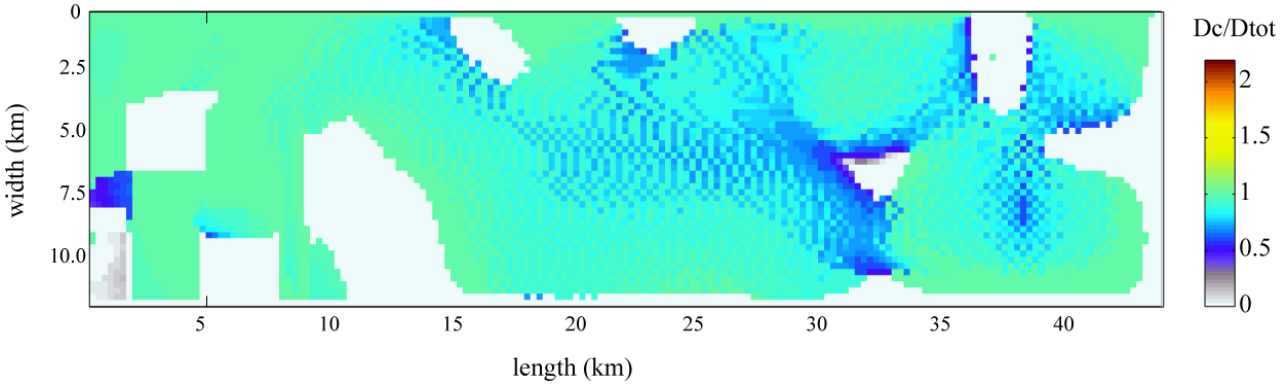

Figure 10

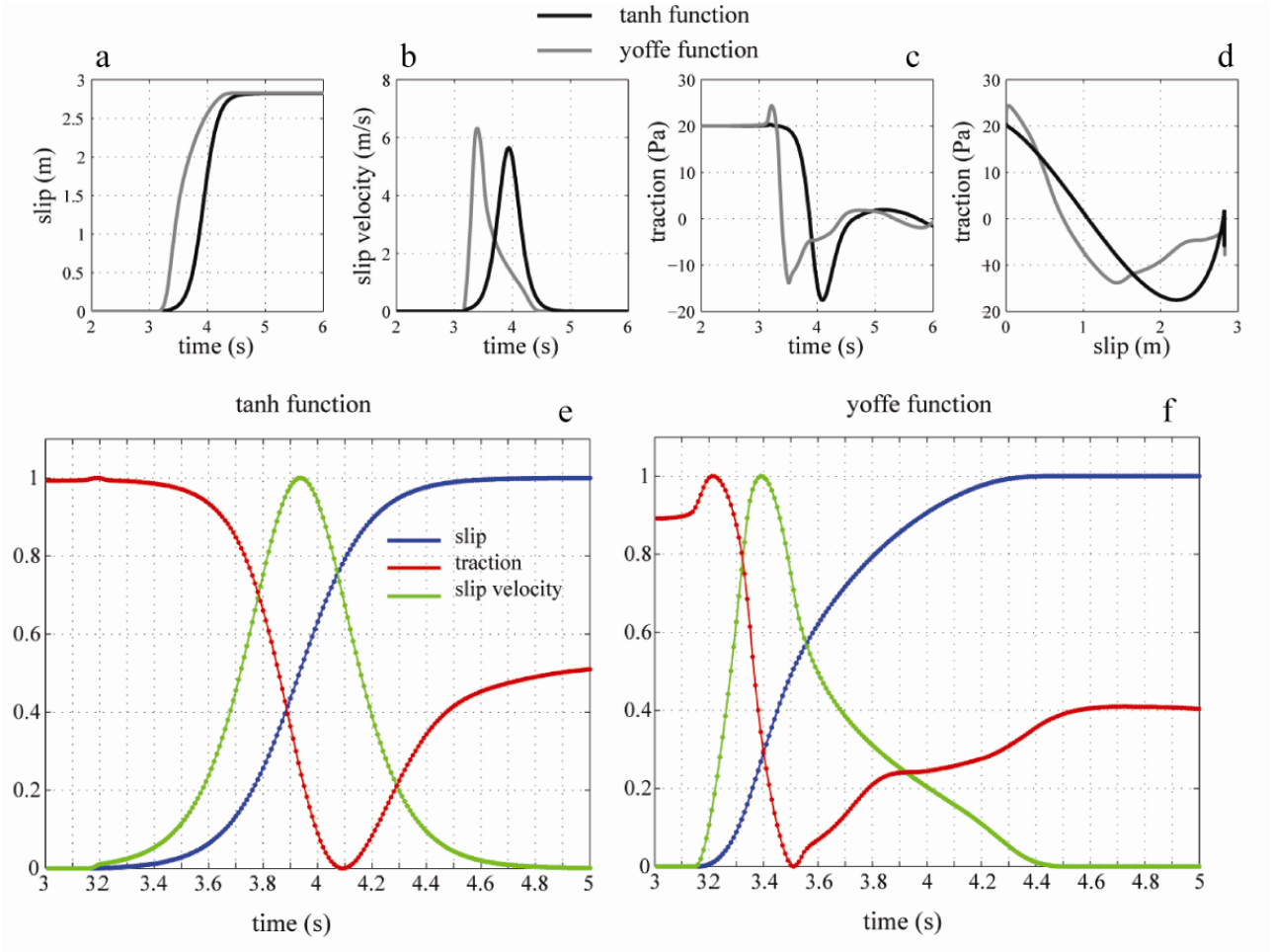
tanh function
yoffe function
a
b
c
d
slip (m)
slip velocity (m/s)
traction (Pa)
traction (Pa)
time (s)
time (s)
time (s)
slip (m)
tanh function
e
yoffe function
f
slip
traction
slip velocity
time (s)
time (s)

Figure 11

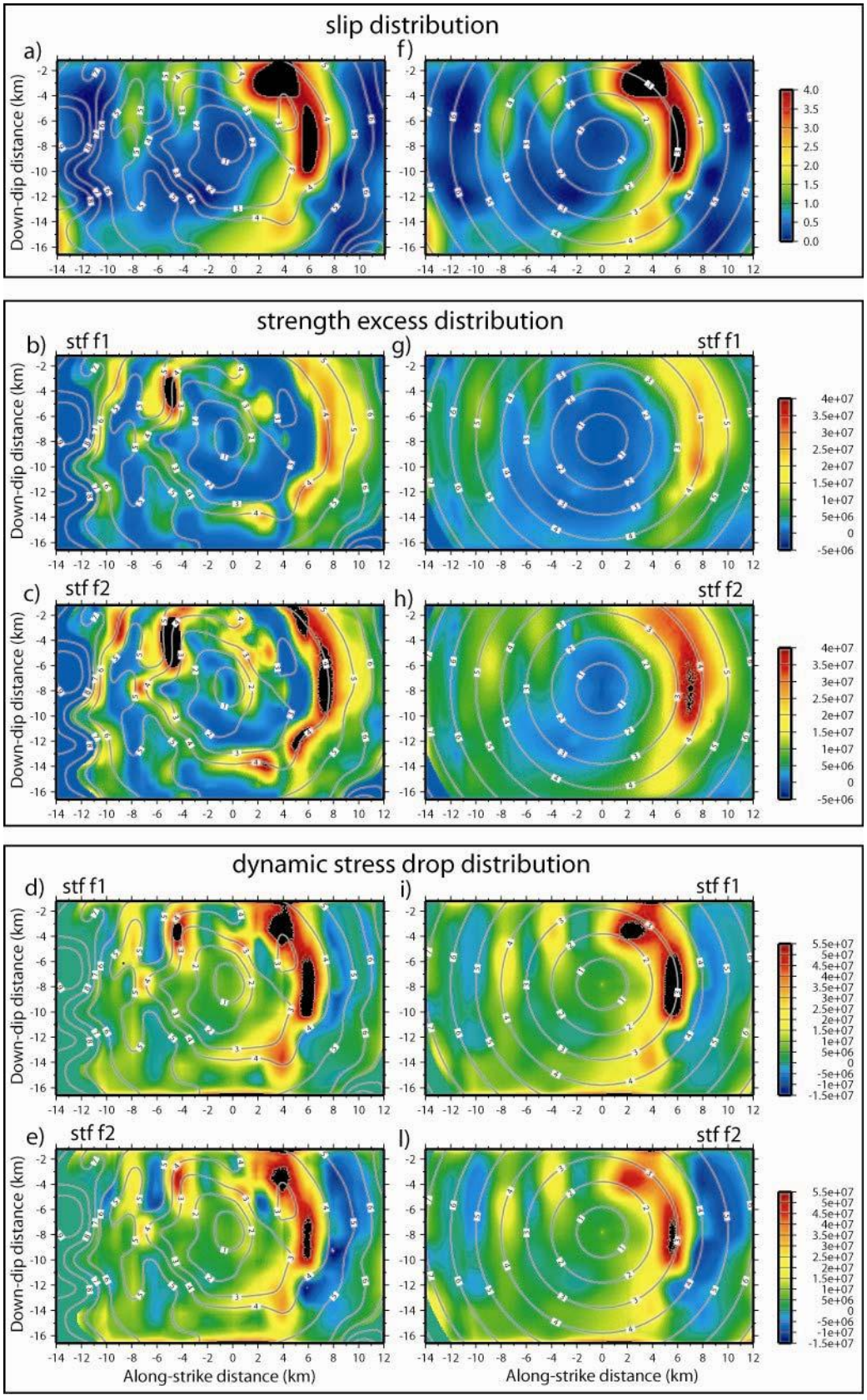
slip distribution
a)
f)
Down-dip distance (km)
4.0
3.5
3.0
2.5
2.0
1.5
1.0
0.5
0.0
strength excess distribution
b)
stf f1
g)
stf f1
c)
stf f2
h)
stf f2
4e+07
3.5e+07
3e+07
2.5e+07
2e+07
1.5e+07
1e+07
5e+06
0
-5e+06
dynamic stress drop distribution
d)
stf f1
i)
stf f1
e)
stf f2
l)
stf f2
5.5e+07
5e+07
4.5e+07
4e+07
3.5e+07
3e+07
2.5e+07
2e+07
1.5e+07
1e+07
5e+06
0
-5e+06
-1e+07
-1.5e+07
Along-strike distance (km)
Along-strike distance (km)

Figure 12

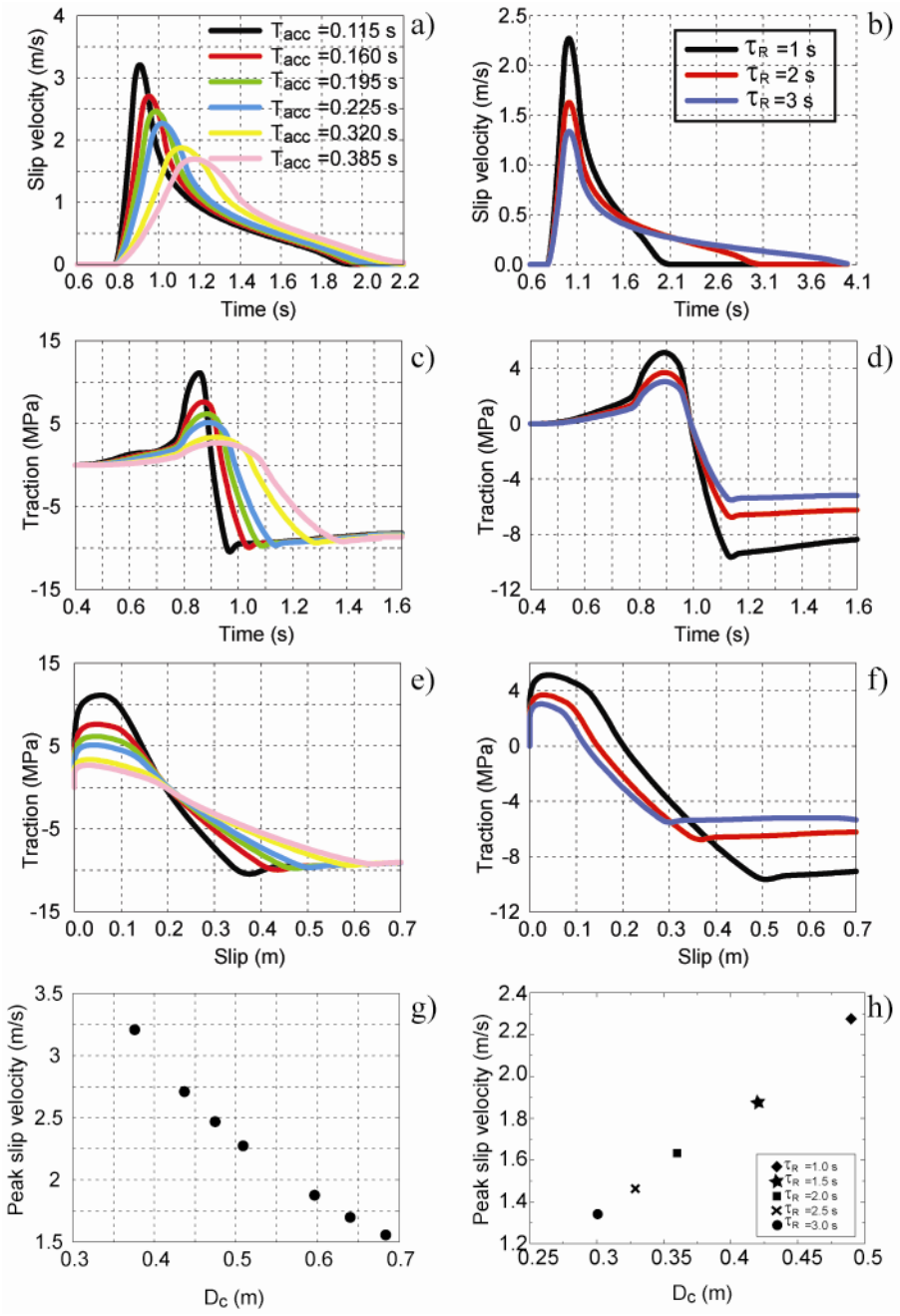

Figure 13

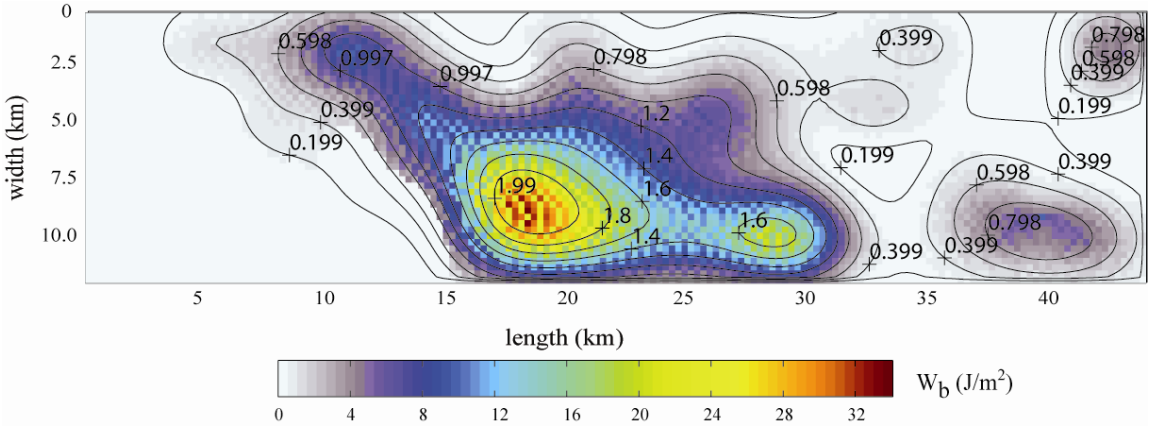

Figure 14